Growth of $ATiO_3$ (A = Ba, Sr) dielectric thin film by a hydrothermal–electrochemical method

2004 J. Phys.: Condens. Matter 16 S1351

(http://iopscience.iop.org/0953-8984/16/14/048)

INSTITUTE OF PHYSICS PUBLISHING JOURNAL OF PHYSICS: CONDENSED MATTER

J. Phys.: Condens. Matter **16** (2004) S1351–S1360 PII: S0953-8984(04)75011-0

Growth of $ATiO_3$ (A = Ba, Sr) dielectric thin film by a hydrothermal–electrochemical method

Koji Kajiyoshi and Kazumichi Yanagisawa

Research Laboratory of Hydrothermal Chemistry, Faculty of Science, Kochi University 2-5-1, Akebono-cho, Kochi-shi 780-8520, Japan

Received 22 January 2004
Published 26 March 2004
Online at stacks.iop.org/JPhysCM/16/S1351
DOI: 10.1088/0953-8984/16/14/048

Abstract

The hydrothermal–electrochemical growth of $ATiO_3$ (A = Ba, Sr) dielectric thin films on Ti substrates in $A(OH)_2$ solutions is reviewed. The film thickness increased monotonically with increase in the quantity of electricity passed through the Ti substrate, and could be controlled coulometrically by this factor. The current efficiency for the film growth was in the range from about 0.6% to 3.0%. (Ba, Sr)TiO_3 solid-solution films could be grown with control of the Ba/Sr composition. $ATiO_3$ thin films could also be grown uniformly on porous Ti bodies using cyclic electrolysis. A tracer experiment revealed that the $ATiO_3$ film grew at the film/substrate interface by transport of both A-site and oxygen atoms from the solution to the interface. The films grown were composed of a thin surface layer having an isotropic polycrystalline structure and an inner layer having a columnar structure. Nanopores were found at the boundaries of columnar grains constituting the inner layer. The observed pores are considered to act as short-circuit paths for mass transport from the film surface to the film/substrate interface. The resistivity of the $BaTiO_3$ thin film was as high as 10^{12} Ω cm in the voltage range up to 2 V. The breakdown field was higher than 30 MV m^{-1}. The dielectric constant and dielectric loss were about 340–350 and 7%–10%, respectively, at 1 kHz and 0.1 V_{rms}. The polarization–voltage hysteresis loops were those of a paraelectric phase.

1. Introduction

Synthesis and growth of complex oxide thin films has been extensively investigated mainly because their electromagnetic properties—such as the ferroelectric, pyroelectric, and piezoelectric properties—are applicable in a tremendous number of microelectronic devices, which include thin film capacitors, ferroelectric memories, pyroelectric detectors, IR imagers, and SAW devices [1–3]. The hydrothermal–electrochemical method is an attractive film-formation technique which makes positive use of hydrothermal and electrochemical reactions

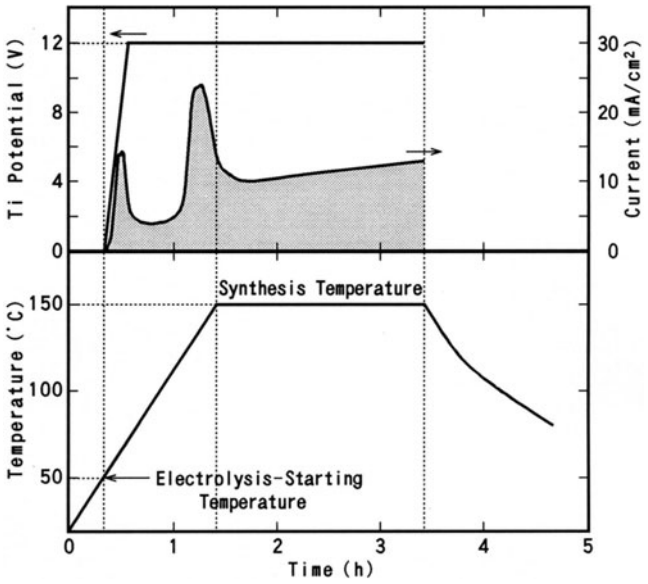

Figure 1. The relation between the temperature profile (lower) and the potentiostatic electrolysis (upper). The potential of the Ti electrode is represented in units of volts versus the Ag/AgCl electrode. The hatched area below the electrolysis current curve corresponds to the quantity of electricity passed.

between a substrate and species included in the synthesis solution [4]. This method permits, for example, a perovskite-type compound ABO_3 to be synthesized on a substrate of B-site metal, oxidized anodically in an aqueous solution containing A-site ions, at temperatures ($\leqslant$ about 200 °C) much lower than those required to obtain crystalline phases in common film-formation techniques such as vacuum evaporation, sputtering, CVD, and the sol–gel method [5–7]. Since this technique utilizes a solution process, it also has a potential advantage over other common film-formation techniques in that thin films can be grown on substrates in any form such as plate, wire, and porous body. The present paper reviews the growth of $ATiO_3$ (A = Ba, Sr) dielectric thin films on Ti substrates in $A(OH)_2$ solutions by this technique.

2. Experimental procedure

Hydrothermal–electrochemical treatments were performed in an autoclave fabricated on the basis of the three-electrode cell arrangement with an Ag/AgCl external reference electrode. A metal substrate and a platinum plate of the same dimensions were suspended as the working and the counter-electrodes, respectively, by 0.5 mm diameter wires of the same metal as the respective electrodes, maintaining a separation of 30 mm between them in the electrolytic cell containing 500 ml of a mixture. Figure 1 shows the relation between the temperature profile (lower) and the potentiostatic electrolysis (upper) used in the hydrothermal–electrochemical treatment. The electrolysis was performed potentiostatically from 50 °C in the heating process to the end of the isothermal process.

Film-constituting phases and their lattice parameters were analysed by x-ray diffractometry (XRD, RINT 1500, Rigaku Denki) under the operating conditions of 40 kV and 100 mA, using Cu Kα radiation with a graphite monochromator and a silicon powder (Si-640b, US Department of Commerce, NIST). The microstructure of the films grown was

investigated using scanning electron microscopy (SEM, S-4000, Hitachi) at an acceleration voltage of 10–20 kV, and by transmission electron microscopy (TEM, H-9000UHR, Hitachi) at an acceleration voltage of 300 kV. Compositional analysis was performed using scanning transmission electron microscopy (STEM, HB501, VG Microscopes) at an acceleration voltage of 100 kV, incorporating energy dispersive x-ray spectroscopy (EDX, KEVEX SUPER8000, Fisons Instruments) with a probe beam of 1 nm diameter and 1 nA current. Depth profiles of the film-constituting elements were investigated by Auger electron spectroscopy (AES, JAMP-7100/E, JEOL). The primary beam parameters used were 5 keV beam energy, 120 nA beam current, 10 μm beam diameter, and 60° angle of incidence. Depth profiles of the oxygen isotopes were generated by secondary-ion mass spectroscopy (SIMS, A-DIDA3000, Atomika) using a 12 keV $133Cs^+$ primary-ion beam with a total current of 150 nA. The depths of the sputtered craters were measured with a mechanical stylus-type surface level monitor (DEKTAK-3030ST, Ulvac Japan). Metal/insulator/metal structures were fabricated by depositing an array of 2.0 mm diameter Ag or Al films on the film surface to measure the electrical properties. Leakage current–voltage characteristics and dielectric breakdown voltages were measured with a voltage–current source (TR6163, Advantest) and with a picoammeter (TR8641D, Advantest). The dependences of the capacitance and dielectric loss on the dc bias voltage and temperature were measured with an LCR meter (HP4284A, Hewlett-Packard). The frequency dependences of the capacitance and dielectric loss were evaluated with an impedance analyser (YHP4194A, Yokogawa-Hewlett-Packard). A ferroelectric tester (RT6000HVS, Radiant Technologies) was used to measure polarization–voltage hysteresis loops.

3. Results and discussion

The electrolysis treatment of this method was modified suitably to grow polycrystalline $SrTiO_3$ thin films on Ti electrodes with accurate control of the film thickness up to about 2 μm [8]. The SEM micrograph in figure 2 shows an about 2 μm-thick $SrTiO_3$ film grown on a Ti substrate by the hydrothermal–electrochemical method with potentiostatic electrolysis at +8.0 V versus Ag/AgCl in 0.5 M $Sr(OH)_2$ solution of pH 14.2 at 150 °C. The film thickness was found to increase monotonically with increase in the quantity of electricity passed through the Ti substrate, and could be controlled coulometrically by this factor [9]. Figure 3 shows the amount of $SrTiO_3$ formed per unit surface area and the corresponding film thickness estimated by gravimetry as a function of the quantity of electricity for various Ti electrode potentials. The other synthesis parameters were kept at the normal values (0.5 M Sr, pH 14.2, and 150 °C). The efficiency increases from 0.6% to 3.0% with decreasing Ti electrode potential, from +16.0 to +8.0 V, versus Ag/AgCl. The current efficiency for the film growth was in the range from about 0.6% to 3.0%, mainly depending on the applied potential and the synthesis temperature. The (Ba, Sr)TiO_3 solid-solution films could also be grown with control of the Ba/Sr composition in aqueous solutions of (Ba, Sr)$(OH)_2$ [10]. Figure 4 shows lattice parameters of cubic $(Ba_ySr_{1-y})TiO_3$ films synthesized in $(Ba_xSr_{1-x})(OH)_2$ solutions. Dotted lines indicate y values estimated from corresponding x values on the basis of Vegard's law. The Ba contents in the solid-solution films are fairly low compared to those in the respective solutions used. It was also confirmed that the $ATiO_3$ thin films can be grown uniformly on the whole surface of porous Ti bodies, by using a cyclic electrolysis in which an anodic potential and a rest potential were applied alternately [11].

The mass transport mechanism during the $ATiO_3$ thin film growth was studied by a tracer technique using ^{18}O [12]. So as to investigate the relations between the atomic orders of incorporation and the resulting in-depth distributions, two kinds of samples were prepared by

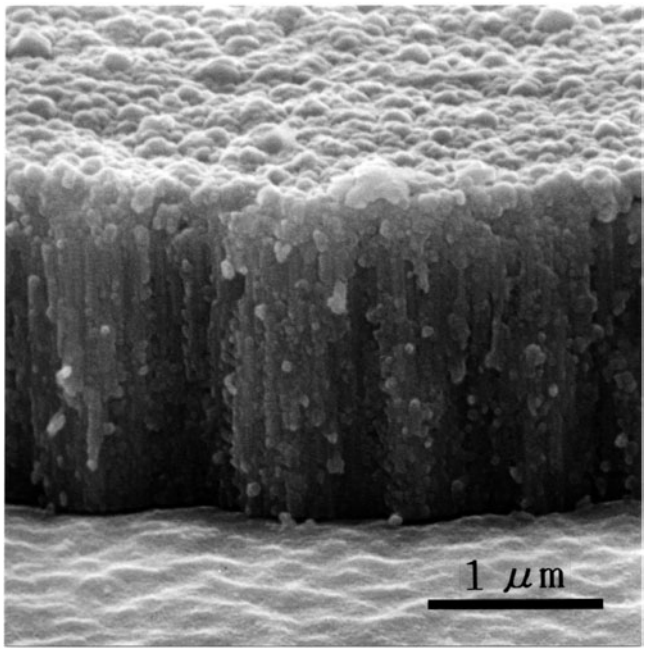

Figure 2. An SEM micrograph of an about 2 μm-thick $SrTiO_3$ film grown on a Ti substrate by the hydrothermal–electrochemical method with potentiostatic electrolysis at +8.0 V versus Ag/AgCl in 0.5 M $Sr(OH)_2$ solution of pH 14.2 at 150 °C.

a sequential treatment process. A sample of the first kind (S5) was grown in the tracer-free solution (the natural abundance was allowed for the ^{18}O tracer) by the initial treatment, and then the film was subsequently grown to an additional thickness in the solution, including the tracer atoms in the subsequent treatment. The second kind of sample (S6) was prepared using these solutions in the reverse order. In order to confirm the homogeneity of natural distributions of ^{18}O and ^{16}O, a reference film of $SrTiO_3$ (S4) was also grown by the single-treatment process in a $Sr(OH)_2$ solution having a natural abundance of the oxygen isotopes. Figure 5 demonstrates SIMS in-depth profiles of the intensity ratio of $^{18}O/^{16}O$ for samples S4, S5, and S6. The difference between S4 and S5 profiles demonstrates that the initial atomic order of incorporation into the growing films is reversed in the films grown. (Similar results were also obtained from a tracer experiment for A-site ions.) Thus, the $ATiO_3$ film was found to grow at the interface between the film and the electrode by transport of both A-site and oxygen atoms from the solution to the interface. Figure 6 symbolically represents the mass transport mode in growing polycrystalline $ATiO_3$ (A = Ba, Sr) film on the basis of the tracer experiment. The left-hand side represents an early stage; those atoms which have been incorporated by this stage are hatched, and those which are to be incorporated are labelled in that order. The right-hand side represents the subsequent stage when the labelled atoms have just been incorporated. The growing interface and its direction are indicated by a hatched line and an arrow, respectively. The transport modes of the elements are intergranular (and/or interstitial) transport of both A and O.

TEM observation revealed that the films grown were composed of a thin surface layer having an invariant thickness of about 0.2 μm and an inner layer that can be grown by the electrolysis [13]. Figure 7 shows a cross-sectional TEM image of a $SrTiO_3$ film grown on a Ti substrate with potentiostatic electrolysis at +8.0 V versus Ag/AgCl in 0.5 M $Sr(OH)_2$

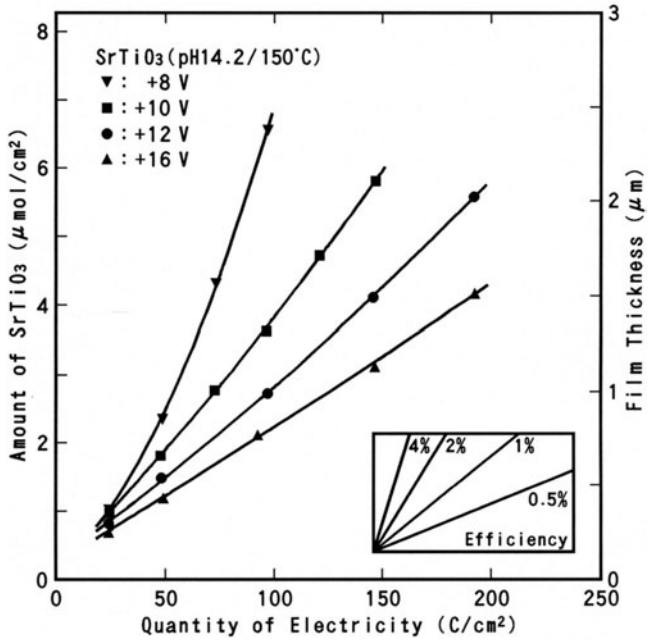

Figure 3. The amount of $SrTiO_3$ formed per unit surface area and the corresponding film thickness estimated by gravimetry as a function of the quantity of electricity for various Ti electrode potentials versus Ag/AgCl. The inset shows slopes corresponding to several typical values of current efficiency. The other synthesis parameters were kept at the normal values (0.5 M Sr, pH 14.2, and 150 °C).

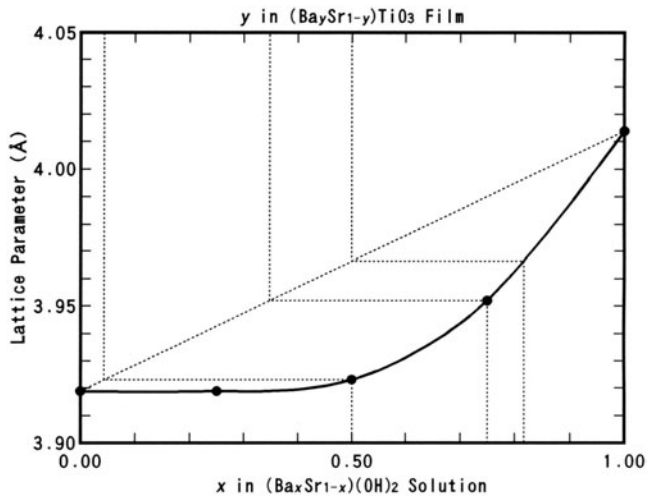

Figure 4. Lattice parameters of cubic $(Ba_ySr_{1-y})TiO_3$ films synthesized in $(Ba_xSr_{1-x})(OH)_2$ solutions. Dotted lines indicate y values estimated from the corresponding x values on the basis of Vegard's law.

solution of pH 14.2 at 150 °C. The cross-section consists of a thin surface layer 0.2 or 0.3 μm thick (layer A) and a thick inner layer having a columnar structure (layer B). The $SrTiO_3$

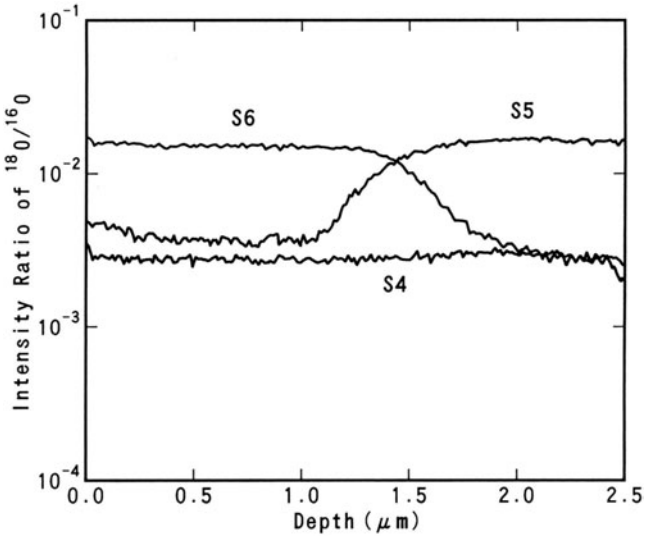

Figure 5. SIMS in-depth profiles of the intensity ratio of $^{18}O/^{16}O$ for samples S4, S5, and S6.

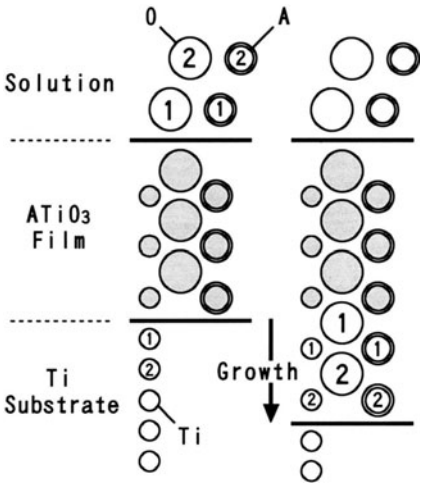

Figure 6. A symbolic representation of the mass transport mode in growing polycrystalline $ATiO_3$ (A = Ba, Sr) film.

grains constituting the surface layer (layer A in figure 7) assume an isotropic polycrystalline structure with a grain size of several tens of nanometres. The surface layer is considered to be re-formed hydrothermally through a dissolution–recrystallization process. Figure 8 shows a magnified TEM image of the $SrTiO_3$ film/Ti substrate interface (interface C in figure 7). Arrows indicate the boundaries of a polycrystalline layer of Ti oxides whose microstructure is different from the columnar one of the overlying, inner $SrTiO_3$ layer. The $SrTiO_3$ grains constituting the inner layer assume an anisotropic structure; they grow into columnar shapes aligning in the columnar structure. The columnar grains measure about 10–30 nm wide and several tens of nanometres to more than 100 nm long. In plan-view TEM images of the $SrTiO_3$ grains constituting the inner layer (layer B in figure 7), the $SrTiO_3$ grains assumed an isotropic

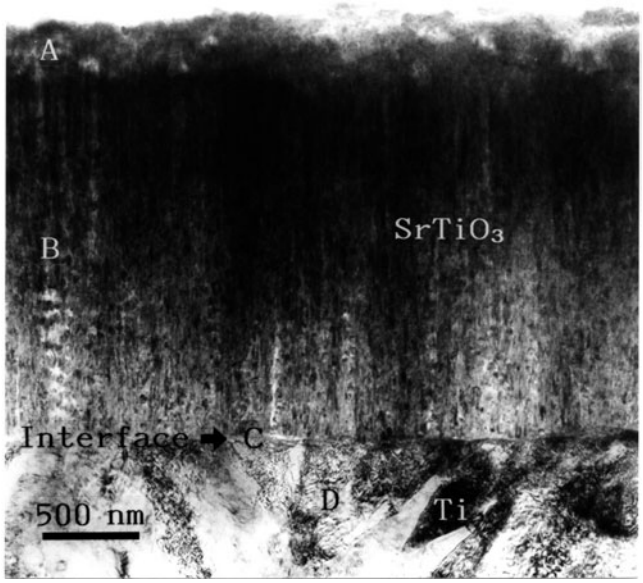

Figure 7. A cross-sectional TEM image of a $SrTiO_3$ film grown on a Ti substrate with potentiostatic electrolysis at +8.0 V versus Ag/AgCl in 0.5 M $Sr(OH)_2$ solution of pH 14.2 at 150 °C.

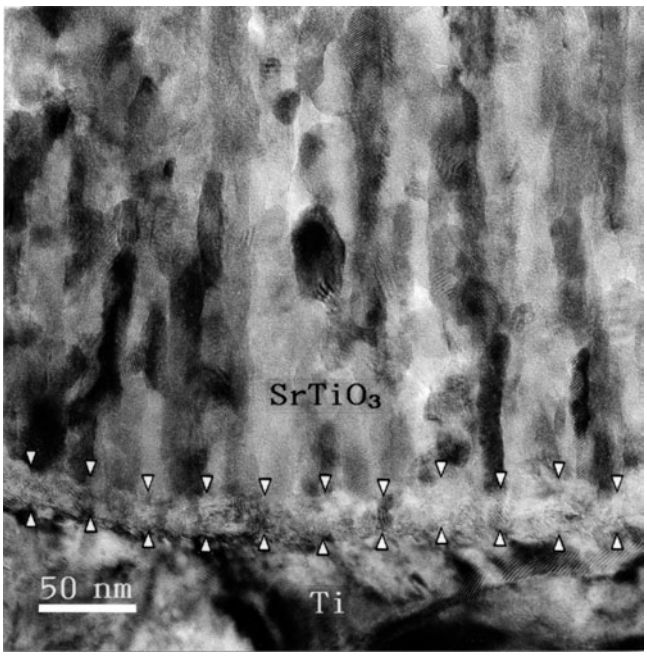

Figure 8. A magnified TEM image of the $SrTiO_3$ film/Ti substrate interface of the $SrTiO_3$ film shown in figure 7.

polycrystalline structure with grain sizes of about 10–30 nm. It should be noted that pores of the order of several tens of nanometres existed at grain boundaries. Such pores were observable

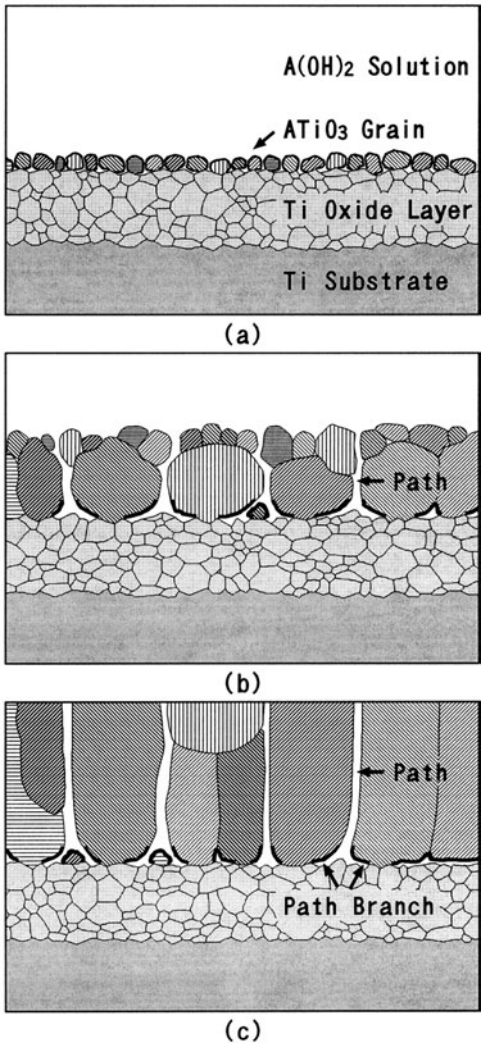

Figure 9. A schematic illustration of the growth process of $ATiO_3$ (A = Ba, Sr) thin film on a Ti oxide layer anodically formed on a Ti substrate by the hydrothermal–electrochemical method.

almost exclusively in the plan-view section; they were rarely observed in the cross-section. The pore is considered to be the cross-section of a short-circuit path extending perpendicularly to the plan-view section, and A-site and O ions are considered to diffuse as solution species through the paths from the film surface to the film/substrate interface.

The film growth mechanism revealed so far is depicted in figure 9. The schematic illustration in figure 9 represents the growth process of $ATiO_3$ (A = Ba, Sr) thin film on a Ti oxide layer anodically formed on a Ti substrate by the hydrothermal–electrochemical method. Bold lines denote those $ATiO_3$ grain surfaces which are growing through a liquid–solid interface reaction:

(a) An initial stage at which the Ti oxide layer has just been covered with $ATiO_3$ crystallites growing at almost all their surfaces.

(b) A next stage at which some of the $ATiO_3$ crystallites have grown to relatively large grains.
(c) The final stage at which columnar $ATiO_3$ grains are growing in a steady state at their bottom surfaces.

A minor contribution of the dissolution–recrystallization process to the grain morphology is neglected.

Electrical measurements were performed on the $BaTiO_3$ dielectric thin film. The resistivity was as high as 10^{12} Ω cm in the voltage range up to 2 V [14]. The breakdown field was higher than 30 MV m^{-1}. The dielectric constant and dielectric loss were about 340–350 and 7% to 10%, respectively, at 1 kHz and 0.1 V_{rms}. The polarization–voltage hysteresis loops were those of a paraelectric phase. These electrical properties indicate that the $BaTiO_3$ thin film is practically applicable in thin film capacitors characterized by dielectric properties with small temperature coefficients.

4. Conclusions

(1) A novel hydrothermal–electrochemical method was developed to prepare $ATiO_3$ thin films uniformly on Ti plate substrates or porous Ti bodies. The film thickness increased monotonically with increase in the quantity of electricity passed through the Ti substrate, and could be controlled coulometrically by this factor.
(2) The mass transport mechanism was revealed by a tracer technique and TEM microscopy. The $ATiO_3$ thin film grows at the film/substrate interface. A-site and O ions diffuse as solution species through open short-circuit paths extending from the film surface to the interface.
(3) The $BaTiO_3$ thin film showed electrical properties such as a dielectric constant of 340–350, a dielectric loss of 7%–10% (1 kHz, 0.1 V_{rms}), resistivity of $\geqslant 10^{12}$ Ω cm ($\leqslant$2 V), and a breakdown voltage of $\geqslant$12 V. The polarization–voltage hysteresis loops were those of a paraelectric phase.

Acknowledgment

The authors would like to express sincere appreciation to Professor Masahiro Yoshimura of the Materials and Structures Laboratory, Tokyo Institute of Technology, for fruitful discussions.

References

[1] Merz W J 1949 The electrical and optical behavior of $BaTiO_3$ single-domain crystals *Phys. Rev.* **76** ([8]) 1221–5
[2] Jona F and Shirane G 1962 *Ferroelectric Crystals* (New York: Pergamon)
[3] Jaffe B, Cook W R Jr and Jaffe H 1971 *Piezoelectric Ceramics* (New York: Academic)
[4] Yoshimura M, Yoo S E, Hayashi M and Ishizawa N 1989 Preparation of $BaTiO_3$ thin film by hydrothermal electrochemical method *Japan. J. Appl. Phys.* **28** ([2]) L2007–9
[5] Feldman C 1955 Formation of thin films of $BaTiO_3$ by evaporation *Rev. Sci. Instrum.* **26** ([5]) 463–6
[6] Feil W A, Wessels B W, Tonge L M and Marks T J 1990 Organometallic chemical vapor deposition of strontium titanate *J. Appl. Phys.* **67** ([8]) 3858–61
[7] Joshi P C and Krupanidhi S B 1992 Strontium titanate thin films by rapid thermal processing *Appl. Phys. Lett.* **61** ([13]) 1525–7
[8] Kajiyoshi K, Tomono K, Hamaji Y, Kasanami T and Yoshimura M 1994 Growth of strontium titanate thin films of controlled thickness by the hydrothermal–electrochemical method *J. Am. Ceram. Soc.* **77** ([11]) 2889–97
[9] Kajiyoshi K, Tomono K, Hamaji Y, Kasanami T and Yoshimura M 1994 Contribution of electrolysis current to growth of $SrTiO_3$ thin film by the hydrothermal–electrochemical method *J. Mater. Res.* **9** ([8]) 2109–17

[10] Kajiyoshi K, Yoshimura M, Hamaji Y, Tomono K and Kasanami T 1996 Growth of (Ba, Sr)TiO_3 thin films by the hydrothermal–electrochemical method and effect of oxygen evolution on their microstructure *J. Mater. Res.* **11** ([1]) 169–83

[11] Kajiyoshi K and Sakabe Y 1999 Preparation of a barium titanate thin film on a porous titanium body by the hydrothermal–electrochemical method *J. Am. Ceram. Soc.* **82** ([11]) 2985–92

[12] Kajiyoshi K, Tomono K, Hamaji Y, Kasanami T and Yoshimura M 1995 Short-circuit diffusion of Ba, Sr, and O during $ATiO_3$ (A= Ba, Sr) thin-film growth by the hydrothermal–electrochemical method *J. Am. Ceram. Soc.* **78** ([6]) 1521–31

[13] Kajiyoshi K, Hamaji Y, Tomono K, Kasanami T and Yoshimura M 1996 Microstructure of strontium titanate thin film grown by the hydrothermal–electrochemical method *J. Am. Ceram. Soc.* **79** ([3]) 613–9

[14] Kajiyoshi K, Sakabe Y and Yoshimura M 1997 Electrical properties of $BaTiO_3$ thin film grown by the hydrothermal–electrochemical method *Japan. J. Appl. Phys.* **36** ([3A]) 1209–15